U.S. DEPARTMENT OF ENERGY

PNNL-23332

Prepared for the U.S. Department of Energy
under Contract DE-AC05-76RL01830

Nanocrystalline SiC and Ti_3SiC_2 Alloys for Reactor Materials: Thermal and Mechanical Properties

CH Henager, Jr.
TJ Roosendaal
BN Nguyen
W Jiang
KJ Alvine
Y Shin
BA Borlaug

April 2014

Pacific Northwest
NATIONAL LABORATORY

Proudly Operated by Battelle *Since 1965*

DISCLAIMER

PACIFIC NORTHWEST NATIONAL LABORATORY
operated by
BATTELLE
for the
UNITED STATES DEPARTMENT OF ENERGY
under Contract DE-AC05-76RL01830

Printed in the United States of America

Available to DOE and DOE contractors from the
Office of Scientific and Technical Information,
P.O. Box 62, Oak Ridge, TN 37831-0062;
ph: (865) 576-8401
fax: (865) 576-5728
email: reports@adonis.osti.gov

Available to the public from the National Technical Information Service
5301 Shawnee Rd., Alexandria, VA 22312
ph: (800) 553-NTIS (6847)
email: orders@ntis.gov <http://www.ntis.gov/about/form.aspx>
Online ordering: http://www.ntis.gov

This document was printed on recycled paper.
(8/2010)

Nanocrystalline SiC and Ti_3SiC_2 Alloys for Reactor Materials: Thermal and Mechanical Properties

CH Henager, Jr.
TJ Roosendaal
BN Nguyen
W Jiang
KJ Alvine
Y Shin
BA Borlaug

April 2014

Prepared for
the U.S. Department of Energy
under Contract DE-AC05-76RL01830

Pacific Northwest National Laboratory
Richland, Washington 99352

Abstract

SiC-polymers (pure polycarbosilane and polycarbosilane filled with SiC-particles) are being combined with Si and TiC powders to create a new class of polymer-derived ceramics for consideration as advanced nuclear materials in a variety of applications. Compared to pure SiC these materials have increased fracture toughness with only slightly reduced thermal conductivity. Future work with carbon nanotube (CNT) mats will be introduced with the potential to increase the thermal conductivity and the fracture toughness. At present, this report documents the fabrication of a new class of monolithic polymer derived ceramics, SiC + SiC/Ti_3SiC_2 dual phase materials. The fracture toughness of the dual phase material was measured to be significantly greater than Hexoloy SiC using indentation fracture toughness testing. However, thermal conductivity of the dual phase material was reduced compared to Hexoloy SiC, but was still appreciable, with conductivities in the range of 40 to 60 W/(m•K). This report includes synthesis details, optical and scanning electron microscopy images, compositional data, fracture toughness, and thermal conductivity data.

Summary

This report documents the synthesis of SiC-based alloys with an overall structure of SiC/Ti_3SiC_2 dual phase composites formed by simultaneous polycarbosilane pyrolysis that forms nanocrystalline SiC and Si + TiC displacement reactions that form $SiC + Ti_3SiC_2$ interpenetrating phase composites. To the best of our knowledge these are the first such dual phase composites made by combining these two methods. The structure and phase morphology of the composites are determined by optical microscopy, scanning electron microscopy, and X-ray diffraction methods. The general microstructural morphology is best described as a blocky, dual phase SiC/Ti_3SiC_2 composite with porosity confined to the SiC phase. Data for thermal conductivity and fracture toughness indicate that properties of these composites are in agreement with what others have measured for similar materials but synthesized by different methods, such as spark plasma sintering, for example. The measured thermal conductivities determined using laser flash thermal diffusivity methods, while preliminary, are in the range of 40 to 60 W/(m•K), which is about half of that for a standard SiC material, such as Hexoloy SiC. This is an expected result since the thermal properties of Ti_3SiC_2 are not as good as SiC. These values are still higher than those typically measured for SiC_f/SiC woven composites, which are often only 20 W/(m•K) or lower. However, the fracture toughness of the SiC/Ti_3SiC_2 composites produced here are significantly increased relative to Hexoloy SiC values. Although fracture toughness is increased it is still insufficient for a structural material and, therefore, the need for textured CNT mats is made evident. Still, this is a very encouraging result and indicates that polymer pyrolysis methods can be used to continue these studies of combining in situ displacement reactions together with CNT mats to make tougher composites than can be synthesized by combining SiC and Ti_3SiC_2 materials alone.

Acknowledgments

The PNNL NEET team would like to acknowledge helpful discussions with Starfire, Inc. and with Shelly Arreguin, UW PhD student studying polymer derived ceramics at PNNL under a NEUP program with Clemson University under Prof. Raj Bordia.

Acronyms and Abbreviations

PNNL	Pacific Northwest National Laboratory
CNTs	Carbon nanotubes
OM	Optical microscopy
SEM	Scanning electron microscopy
EDS	Energy dispersive X-ray spectroscopy
XRD	X-ray diffraction
CVI	Chemical vapor infiltration
SiC	Silicon carbide

Contents

Abstract iv
Summary v
Acknowledgments vi
Acronyms and Abbreviations vii
Figures ix
Tables x
1.0 Introduction 1
1.1 Research Background 1
1.1.1 Fracture Toughness and Thermal Conductivity 2
1.1.2 Radiation Damage Resistance 3
2.0 Synthesis of SiC Alloys with Ti_3SiC_2 4
3.0 Characterization of SiC Alloys with Ti_3SiC_2 5
3.1 Optical Microscopy (OM) 6
3.2 Scanning Electron Microscopy (SEM) 8
3.3 X-ray Diffraction (XRD) 10
3.4 Density 10
3.5 Thermal Conductivity 10
3.6 Fracture Toughness 11
4.0 Conclusions 12
5.0 References 15

Figures

Figure 1. A gel cast mixture of polycarbosilane polymer filled with 30-vol% SiC-particles and then filled with 40-vol% Si + TiC powders and cured at 60˚C. This creates a smooth solid green disk that can be handled and machined. The smaller disk on the left is a 1-inch diameter (2.54 cm) that is used for hot pressing while the larger disk on the right is 2 inches (5.08 cm) in diameter for future use. 4

Figure 2. XRD data from cured and pyrolyzed polycarbosilane polymer materials, SMP-10 (pure polymer) and SL-MS30 (SiC-filled polymer). The filled polymer contains 45-nm sized SiC-particles at 30-vol% and the XRD data reflects this for both the cured and pyrolyzed conditions. In contrast, the pure polymer is glassy as cured and crystallizes with an average SiC size of 46.5-nm at 1600˚C (1873 K). 5

Figure 3. Ternary isotherm section of Ti-Si-C system at 1250˚C (1523 K). The 3:2 mole ratio of Si:TiC (connected by the dashed line) reacts to give composition marked as TSC1 on this diagram, which is on the join between SiC and Ti_3SiC_2. Overall, this diagram indicates that the four phases SiC, TiC, Ti_3SiC_2, and $TiSi_2$ are expected to occur in this SiC-alloy system at equilibrium. 7

Figure 4. Optical micrograph showing SiC/Ti_3SiC_2 interpenetrating phase microstructure visible in several large colonies surrounded by porous SiC-polymer pyrolysis dark grey regions. The light grey platelets in the large white particles are the SiC that forms during the displacement reaction between Si and TiC. This sample was hot-pressed at 1550˚C (1823 K) in argon. 7

Figure 5. Optical micrograph of hot-pressed SiC-alloy at 1800˚C and 20 MPa. The SiC-platelet features in Fig. 4 are no longer present but are replaced by a more blocky SiC/Ti_3SiC_2 phase structure. The light grey phase is Ti_3SiC_2 and the darker grey phase is SiC, both from the displacement reaction and from the polymer pyrolysis plus the SiC-filler. SiC alignment within the Ti_3SiC_2 matrix is still evident. 8

Figure 6. SEM images of a SiC-alloy hot pressed at 1800˚C (2073 K) and 20 MPa pressure from SiC-filled polymer plus Si + TiC powders at 63% powder loading. The white phase is the Ti_3SiC_2 phase and the darker grey phase is SiC. Note that the pores are contained entirely within the SiC phase. 9

Figure 7. XRD data from each of the samples listed in Table 2. Residual TiC is observed in some of the samples but the major phases are SiC and Ti_3SiC_2 as shown. 10

Figure 8. Thermal conductivity data from Ref. [38] showing the effects of adding SiC to Ti_3SiC_2 to increase its thermal conductivity. PNNL average thermal conductivity data for the six nominally identical specimens in Table 2 is shown in blue on this graph and corresponds quite well with this published data at higher temperatures. 11

Figure 9. Measured fracture toughness from each of the samples from Table 2 as determined using the indentation fracture toughness method. Ten indents were used for each data point shown in the figure. All of the samples showed an increase in toughness as compared to Hexoloy SiC, which was also tested in this dataset. The dashed green line shows the Hexoloy toughness. 12

Figure 10. Plot of thermal conductivity as a function of sample density. There is a slight negative correlation between density and conductivity that is unexpected. For the most part, however, this plot shows a lack of a strong correlation since the fitted line has a correlation factor less than 0.3. 13

Figure 11. Plot of fracture toughness (indentation method) as a function of sample density. Compared to the lack of correlation for the thermal data this dataset does indicate a general improvement of toughness with increasing density, which would be expected as porosity is decreased. 13

Tables

Table 1 – Research and Use Issues for SiC-based Materials as Nuclear Reactor Materials 2

Table 2. Basic Property Data for Hot-Pressed Nanocrystalline SiC and Ti_3SiC_2 Dual Phase Materials 5

Table 3. Average of EDS data for SiC and Ti_3SiC_2 phases from SEM data 8

1.0 Introduction

1.1 Research Background

SiC and SiC-based composites have been investigated for several years as candidate structural and insulator materials for fusion energy systems [1-10]. Early SiC-based fibers for SiC-composites were found to be unstable under irradiation [11], but more mature SiC-fibers have emerged as a successful nanocrystalline SiC engineered material polymerized from high-purity polymers and e-beam crystallized [1, 12]. SiC-based composites have thus emerged as a promising structural material for fusion energy systems, including first wall and breeder-blanket materials. Joining, thermal conductivity, and gas permeation remain as engineering issues for this application. While SiC-based composites, such as the continuous, Hi-Nicalon Type S fiber, 2D woven, chemical vapor infiltration (CVI)-SiC materials [1, 2], may have a place in advanced reactors, the gas permeability and thermal conductivity issues do not allow some critical applications. A dense SiC-based material system with high thermal conductivity and small impurity diffusion coefficients is required for this and other critical reactor materials applications. However, monolithic SiC has low fracture toughness and cannot be considered without some reinforcement phase. This report documents part of an extensive effort in developing such SiC-based composite materials for these applications. The critical issues that require resolution in order for new SiC-based materials to be considered for advanced reactor uses are 1) fracture toughness, 2) radiation damage, 3) thermal conductivity, and 4) fission product mobilities. Moving away from expensive fibers and CVI synthesis provides a low-cost synthesis method that is an additional advantage.

Overall radiation damage tolerance and swelling at low temperatures is considered an issue for using SiC-based materials at 573 K, which is the temperature range for conventional light water reactors. The vast majority of the data indicates that swelling in SiC is significant at these temperatures, saturating at about 2% swelling [13]. Thermal conductivity is also degraded at these irradiation temperatures, decreasing to about 10 W/(m•K) or less at 573 K irradiations [13, 14] due to an accumulation of point defect damage. These data suggest that it is far better for SiC-based materials to operate at higher temperatures in terms of property degradation. For example, at 1073 K irradiation swelling in SiC is less than 1% and thermal conductivity is upwards of 20 W/(m•K).

Increasing the operating temperature by at least 200 K over current operating temperatures results in improved performance for SiC-based materials, and the incorporation of carbon nanotubes (CNTs) should alleviate the thermal conductivity issues that are of concern for many nuclear applications of SiC. Moving away from expensive SiC-fibers to CNTs may also reduce manufacturing costs since CNTs are becoming more of a commodity item. Others have shown remarkable improvements in materials properties using CNTs of varying types [15].

Therefore, the issues of 1) radiation damage tolerance and swelling at low temperatures, 2) thermal conductivity, and 3) capability of low-cost synthesis methods are classified as problematic to SiC in general and are specifically addressed in this research by advocating higher use temperatures, CNTs for improved thermal conductivity, and also for lower cost synthesis methods. The proposed material, then, is not a fiber-reinforced composite material with the associated high cost of fiber and gas permeability issues [13]. However, moving away from continuous fiber reinforced material exposes the low fracture toughness of SiC, while at the same time making a gas impermeable material possible via near-theoretical dense processing. The critical issue then becomes fracture toughness as long as the irradiation temperature exceeds about 1000 K. Table 1 lists the various issues facing SiC-based materials with suggested approaches to resolve them.

Table 1 – Research and Use Issues for SiC-based Materials as Nuclear Reactor Materials

Issue	Description	Resolution
Radiation Damage/Swelling	Swelling is significant below 1173 K but saturates at low doses.	Nanocrystalline SiC/Ti_3SiC_2 with CNT reinforcement may have superior damage resistance. Operating temperatures adequate to 1700 K to avoid peak swelling.
Thermal Conductivity	Radiation damage creates large phonon scattering, reduces K_{th} especially for SiC-fiber composites made by CVI.	Avoid porous fiber composite CVI architecture with all the internal interfaces, add CNTs with superior K_{th}, operate above 823 K.
Gas Permeable	Porous SiC-fiber composites by CVI are highly gas permeable.	Avoid CVI architecture. Near theoretical dense nanocrystalline composites will be gas impermeable.
Fracture Toughness	Monolithic SiC is brittle material; continuous SiC-fiber materials have requisite toughness, with strong R-curve.	Design tough nanocomposite using Ti_3SiC_2-phase reinforcement plus CNT mechanical reinforcement with 3D texture.
Fission Product Diffusion	Micro-cracks and pores in CVD SiC allow radionuclide ^{110m}Ag to migrate and potentially to release to the environment.	SiC/Ti_3SiC_2 + CNT may block the diffusion pathway by eliminating the micro-cracks interconnected with pores.
Lower Cost Synthesis	Continuous SiC-fiber composites made by CVI have high costs due to high cost of fiber.	SiC/Ti_3SiC_2 + CNT composites will have reduced processing costs compared to SiC-fiber composites.

1.1.1 Fracture Toughness and Thermal Conductivity

While continuous fiber reinforced SiC-composites do have adequate fracture toughness via the well-understood debonding fiber toughening mechanics, an approach using CNTs to improve both properties requires some additional justification. One novel approach is using CNT mats that are textured in 3D using new imprinting techniques to achieve more substantial toughening compared to untextured CNT mats or to dispersed CNTs within SiC/Ti_3SiC_2 nanocomposites. To the best of our knowledge, this approach has not been tried yet by other researchers and clearly represents a new approach to composite toughening using CNTs. With regard to fracture toughness and thermal conductivity, a SiC/Ti_3SiC_2 + CNT nanocrystalline composite could have adequate properties if well designed. Three different mechanisms are being investigated to improve fracture toughness in these nanocrystalline composites. One is through the use of SiC/Ti_3SiC_2 composite toughening that makes use of the intrinsic toughness of Ti_3SiC_2-phase materials. The second is the use of CNT toughening mechanics. Thirdly, the overall 3D architecture of the CNT mats can provide energy absorption and enhanced fracture toughness.

Prior work at PNNL has demonstrated that solid-state displacement reactions between TiC and Si lead to several tough alloys consisting of Ti_3SiC_2 and SiC [16, 17]. A displacement reaction occurs when two (or more) materials are combined and undergo a simultaneous reaction to produce two (or more) product phases. The displacement reaction between Si + TiC produces SiC + Ti_3SiC_2 in an interpenetrating phase

morphology. The two product phases often interpenetrate since they form via short-range diffusion simultaneously and, therefore, remain proximate during the reaction. The phase morphology produced by the Si + TiC reaction consists of SiC-platelets aligned within blocky Ti_3SiC_2 grains, which contributes to an intrinsic toughening. PNNL-produced SiC/Ti_3SiC_2 composite materials exhibit a K_{IC} toughness of almost 10 MPa√m without further optimization. The increased toughness is attributed to the intrinsic toughness of the Ti_3SiC_2 phase, one of the so-called MAX phase layered ceramic structures [17-22], which grows in an interpenetrating manner with the SiC phase during the displacement reaction. In addition, the growth during displacement reaction processing provides a highly aligned microstructure that enhances this toughness. The addition of CNTs, as either individual entities or as textured 3D mats, will also enhance the fracture toughness compared to monolithic SiC [13]. The 3D texturing effect is more difficult to quantify without additional data, however the energy absorption due to CNT straightening and interlocking, as well as crack deflection and tortuosity will achieve additional toughening compared to simple CNT dispersions in a SiC-matrix. The goal is to synthesize a material with a K_{IC} toughness of at least 15-20 with a substantial R-curve response, and it is anticipated that the 3D texturing will help achieve this toughness increase.

CNTs have been shown to increase thermal properties for almost all materials that they can be distributed in [23-26]. The results of small additions of CNTs to polymers, for example, lead to thermal conductivity increases of up to 60% depending on the loading and on the type of CNT. Additions of CNTs to conventional C-fiber-reinforced SiC-composites also indicate improved thermal conductivity [23]. This is significant because present SiC_f/SiC composites are borderline for thermal conductivity for nuclear applications and this critical property only degrades under irradiation [13].

1.1.2 Radiation Damage Resistance

Although SiC has excellent radiation damage resistance it is not immune to radiation damage processes. Under 2 MeV Au^{2+} ion irradiation at room temperature, nanostructured high-purity 3C-SiC, composed of 4.6-nm crystallites, was fully amorphized at a dose comparable to the amorphization dose for bulk SiC [27]. The behavior can be attributed to high ion flux and sluggish migration of point defects within the SiC grain interior. Amorphization in nanocrystalline 3C-SiC is likely to arise from local defect accumulation and interaction within the interior of grains, leading to a catastrophic disruption and collapse of the crystal structure, quite similar to the processes in ion-irradiated bulk single-crystal SiC. Recent results [28] have revealed that, under identical irradiation conditions with Si^+ ions, full amorphization of 3C-SiC with grain sizes ranging from 2.0 – 3.8 nm requires a lower dose than for single crystal 3C-SiC. The average size of the 3C-SiC crystallites, observed from the (111) plane diffraction, decreased nonlinearly from 3.8 nm for an unirradiated sample to 1.5 nm for a fluence of 12 Si^+/nm^2 at room temperature, and further decreased until the material was fully amorphized at 0.24 dpa. This behavior has been attributed to interface amorphization during the ion irradiation. Recent results [29] indicate that although nanograins of SiC can be readily amorphized under ion irradiation below 500 K, nanograins at 550 K grow to larger sizes; furthermore, the grain size tends to saturate at a high fluences [29]. The observed sharp transition from irradiation-induced interface-driven amorphization at 500 K to crystallization at 550 K is an indication of the structural stability of the nanostructured SiC under ion irradiation. Clearly, more research efforts are needed to study the higher-dose behavior of nanocrystalline SiC as well as to understand the physical processes.

2.0 Synthesis of SiC Alloys with Ti_3SiC_2

SiC-based alloys are being synthesized using a commercial polycarbosilane polymer consisting of either pure polycarbosilane or polycarbosilane filled with SiC-particles[1], with added Si and TiC powders. The materials are combined at maximum powder loading amounts, which is typically about 70% by volume. The Si powders are 99.995% purity and less than 10-µm in diameter. The TiC powders are 99.95% purity and 2-µm in diameter. The Si and TiC powders are combined using ball mixing for 16 h using zirconia balls as the mixing media at low mixing rates of 30 to 40 RPM. The polymers are then added to the mixed Si + TiC powders and further ball-mixed under inert atmospheres for an additional 16 h followed by 20 min sonication step for suspending the powders in the liquid prior to gel casting. The liquid slurries are then cured at 60˚C for several hours to several days in an inert gas oven. This forms a green solid disk that is suitable for further processing, such as hot pressing (See Figure 1). The pure polycarbosilane requires several days to cure whereas the polymer filled with SiC-particles (SL-MS30) requires only a few hours.

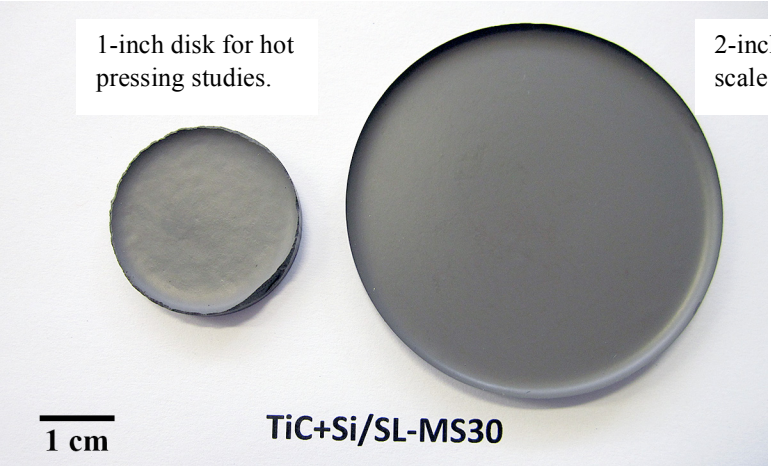

Figure 1. A gel cast mixture of polycarbosilane polymer filled with 30-vol% SiC-particles[2] and then filled with 40-vol% Si + TiC powders and cured at 60˚C. This creates a smooth solid green disk that can be handled and machined. The smaller disk on the left is a 1-inch diameter (2.54 cm) that is used for hot pressing while the larger disk on the right is 2 inches (5.08 cm) in diameter for future use.

X-ray diffraction (XRD) and differential thermal analysis (DTA) were used to study the pyrolysis of these polymers, which can be fully crystallized above 1550˚C (1823 K). The XRD data after heating to 1600˚C (1873 K) is shown in Figure 2 and confirms that nanocrystalline SiC is formed. The filled polymer material has crystalline SiC-particles about 45-nm in size as fillers and those are seen in the XRD spectrum after curing, while the pure polymer appears to be fully amorphous after curing and does not contain any crystalline SiC phase. Although both polymers were investigated during this initial study, it proved easier to work with the filled polymer system, the SL-MS30, so the remained of this report discusses that particular system together with the added Si + TiC powders.

The cured green disks were smoothed to remove the edges formed from the molding step, wrapped in graphite paper (Grafoil) and hot-pressed in a graphite die at 1800˚C (2073 K) and 20 MPa for 2 h. The disks were typically 3-mm in thickness and consolidated to 2-mm thick after hot pressing.

[1] Starfire Systems, Inc., Schenectady, NY
[2] SL-MS30 is a Starfire designation referring to 30-vol% SiC-particulate filled polycarbosilane

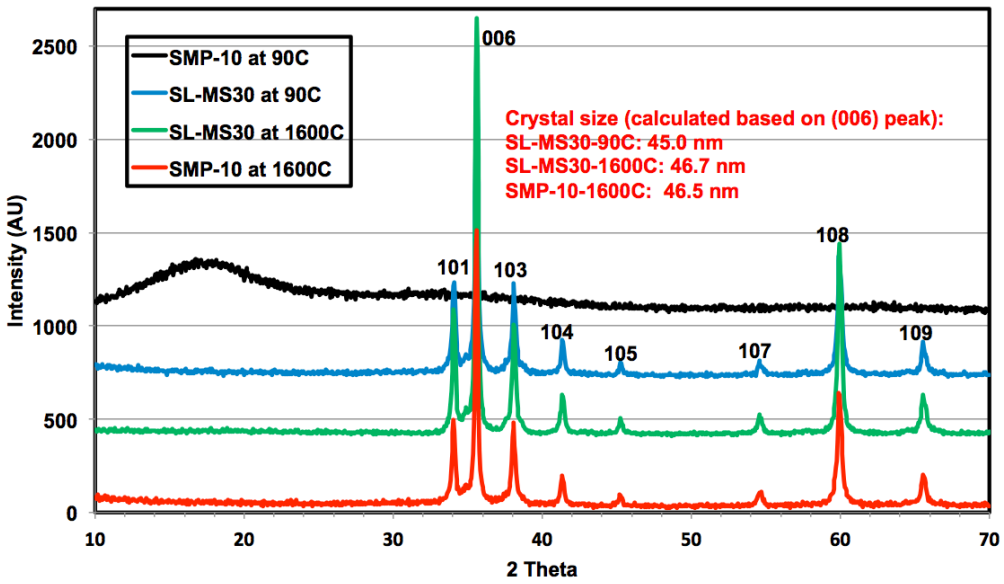

Figure 2. XRD data from cured and pyrolyzed polycarbosilane polymer materials, SMP-10 (pure polymer) and SL-MS30 (SiC-filled polymer). The filled polymer contains 45-nm sized SiC-particles at 30-vol% and the XRD data reflects this for both the cured and pyrolyzed conditions. In contrast, the pure polymer is glassy as cured and crystallizes with an average SiC size of 46.5-nm at 1600˚C (1873 K).

3.0 Characterization of SiC Alloys with Ti_3SiC_2

Hot-pressed samples in the form of thin disks were fabricated as discussed above and were characterized using optical and scanning electron microscopy, density via Archimedes method, thermal conductivity using laser flash methods, and fracture toughness using indentation methods. The disks were prepared for laser flash conductivity measurements by polishing them to a 1-µm surface finish using diamond-polishing cloths. The disks were also used for the density measurements but were then sectioned and polished in cross-section for the microscopy studies, XRD, and indentation fracture toughness testing. Table 2 lists the major results from the characterization work to date.

Table 2. Basic Property Data for Hot-Pressed Nanocrystalline SiC and Ti_3SiC_2 Dual Phase Materials

Sample I.D.	ρ (g/cm^3)	K_{Th} @ 25˚C $(W/(m*K))$	K_{Th} @ 300˚C $(W/(m*K))$	K_{Th} @ 500˚C $(W/(m*K))$	Ti-Phase (%)	K_c $(MPa*m^{0.5})$
Hexoloy SiC	**3.10**	**113.3**	**78.6**	**66.9**	**–**	**4.6**
S30-TSC57-HP-T18-052	3.79	56.1	42.0	39.0	–	4.7
S30-TSC57-HP-T18-053	3.66	26.0	33.6	–	–	4.8
S30-TSC60-HP-T18-060	3.83	49.2	63.5	59.6	39.2%	5.0
S30-TSC63-HP-T18-079	3.83	18. 8	32.6	35.2	44.4%	7.5
S30-TSC63-HP-T18-080	3.81	39.6	37.7	36.0	36.8%	5.4
S30-TSC63-HP-T18-089	3.80	29.0	28.1	28.4	31.5%	5.2
S30DCP-TSC63-HP-T18-093	4.03	20.2	24.2	26.1	-	5.7
S30DVB-TSC63-HP-T18-094	4.03	23.6	27.0	28.1	-	5.8

The densities of the hot-pressed materials, with the exception of Samples 093 and 094 that were gelled with catalytic amounts of dichlorophenol (DCP) and divinylbenzene (DVB), approach the theoretical density of solid bodies that are 50% SiC and 50% Ti_3SiC_2, which is 3.87 g/cm^3. The majority of the samples produced contain significant porosity that appears to be related to the inability of the hot press to achieve higher pressures during hot pressing. Note that the fracture toughness values are all above that of Hexoloy SiC but that measured thermal conductivities are lower.

3.1 Optical Microscopy (OM)

Optical microscopy (OM) was used to image the samples from 50x to 500x with a DIC prism in order to observe the phase morphologies, determine porosity, and perform simple stereological measurements. In some cases these images can be used to provide phase areal fractions. The main findings from the OM data presented here is that the SiC-alloy has been synthesized and consists of a porous SiC phase and a dense Ti_3SiC_2 phase having an overall microstructure consistent with an annealed displacement reaction structure. The porosity is apparently due to the fact that the hot pressing is being performed at a pressure that is too low to allow densification of the filled polymers. The presence of porosity in the SiC phase will, of course, affect the measured thermal conductivity.

To help understand the phases that are in the OM images, Figure 3 shows the phase diagram for the ternary Ti-Si-C system that is appropriate for the SiC-based alloys being synthesized using SiC-polymers and Si + TiC powders. These react together to form SiC from the polycarbosilane plus SiC + Ti_3SiC_2 from a displacement reaction between the Si and TiC. Previous work at PNNL using these reactions to form interpenetrating phase composites [17, 30] in a variety of systems involving metal carbides and Si and on joining SiC using Si + TiC [31-35] has resulted in a deep understanding of the microstructure formation during these complex reactions [36, 37].

Figure 4 shows one of the early results from hot-pressing the pure SiC polymer, polycarbosilane, filled with Si + TiC powders at 1550˚C in argon. The characteristic dual phase observed in the large white particles is due to the simultaneous growth of SiC as platelets oriented within the Ti_3SiC_2 matrix phase. The two phases form together as the Si + TiC displacement reaction occurs due to coupled diffusion at elevated temperatures [36, 37]. The darker grey regions are the SiC phase from the polycarbosilane pyrolysis. Some porosity is also visible in the image. XRD studies have shown that better yield of crystalline SiC is obtained at higher temperatures and that hot pressing at temperatures higher than 1550˚C would also give higher overall densities. It was also decided to work with the SiC-filled polymer, denoted as SL-MS30, since higher ceramic yields are achievable. Overall, the amount of Si + TiC powder loading is then reduced but the total powder loading is maximized when considering the total of SiC + Si + TiC loading. Green curing time is also reduced and much higher densities are obtained.

Figure 5 shows a typical hot-pressed microstructure following hot pressing at 1800˚C (2073 K) and 20 MPa pressure in graphite dies under vacuum. At 1800˚C the displacement reaction microstructure is best described as blocky SiC dispersed within and around a larger grained Ti_3SiC_2 phase.

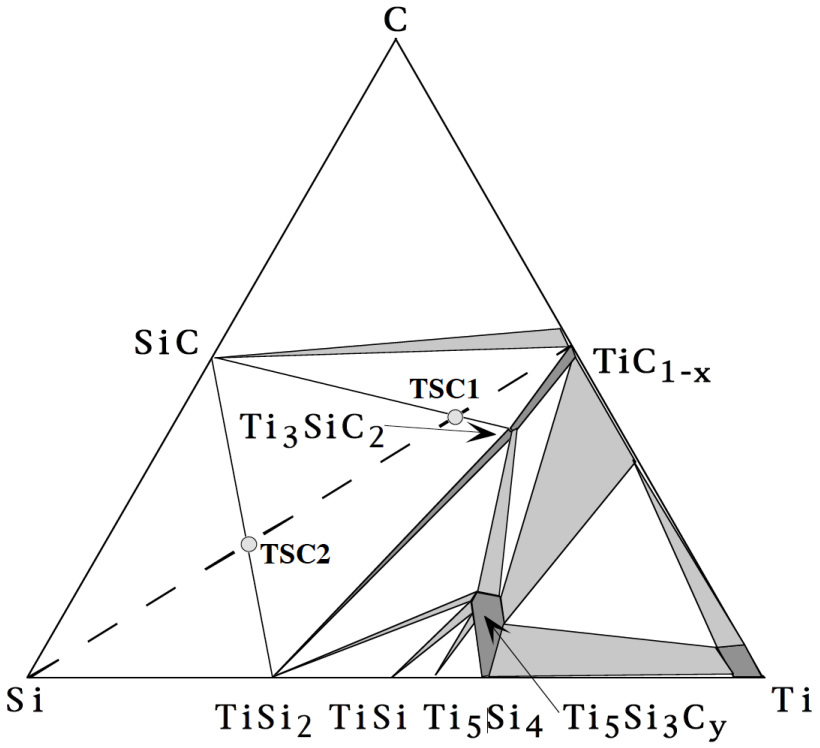

Figure 3. Ternary isotherm section of Ti-Si-C system at 1250˚C (1523 K). The 3:2 mole ratio of Si:TiC (connected by the dashed line) reacts to give composition marked as TSC1 on this diagram, which is on the join between SiC and Ti_3SiC_2. Overall, this diagram indicates that the four phases SiC, TiC, Ti_3SiC_2, and $TiSi_2$ are expected to occur in this SiC-alloy system at equilibrium.

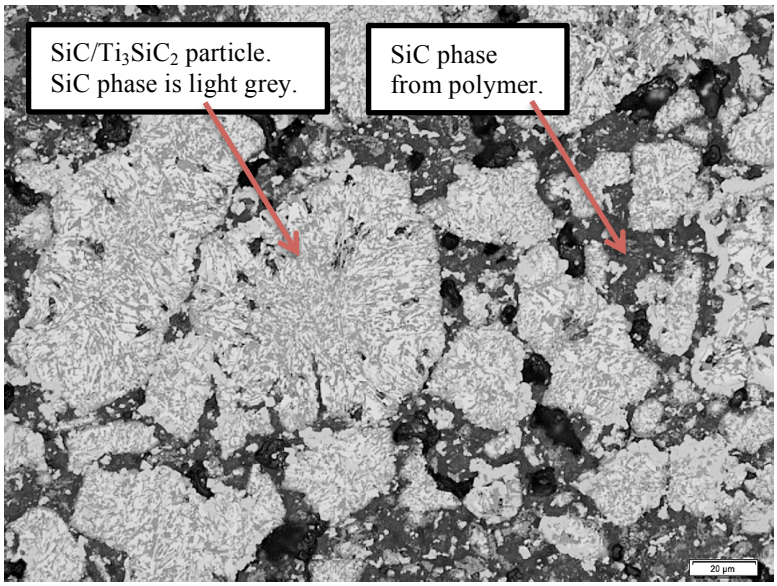

Figure 4. Optical micrograph showing SiC/Ti_3SiC_2 interpenetrating phase microstructure visible in several large colonies surrounded by porous SiC-polymer pyrolysis dark grey regions. The light grey platelets in the large white particles are the SiC that forms during the displacement reaction between Si and TiC. This sample was hot-pressed at 1550˚C (1823 K) in argon.

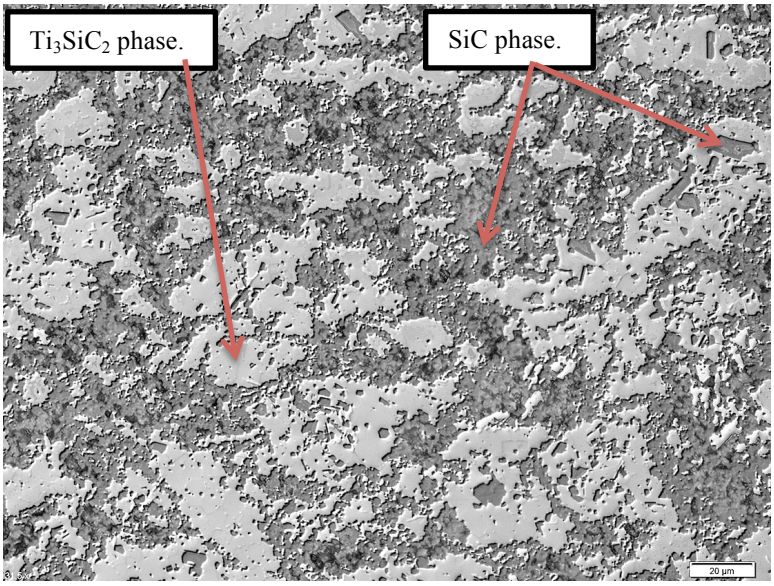

Figure 5. Optical micrograph of hot-pressed SiC-alloy at 1800˚C and 20 MPa. The SiC-platelet features in Fig. 4 are no longer present but are replaced by a more blocky SiC/Ti_3SiC_2 phase structure. The light grey phase is Ti_3SiC_2 and the darker grey phase is SiC, both from the displacement reaction and from the polymer pyrolysis plus the SiC-filler. SiC alignment within the Ti_3SiC_2 matrix is still evident.

3.2 Scanning Electron Microscopy (SEM)

Scanning electron microscopy (SEM) was performed to obtain higher magnification images as well as perform energy dispersive X-ray spectroscopy (EDS) for compositional information in conjunction with X-ray diffraction (XRD). The SEM images reveal information that is not observed in the OM images and also provide detailed spatial compositional information. Figure 6(a-c) show a sequence of SEM images of increasing magnification of the sample shown in Fig. 5 and reveal 1) the Ti_3SiC_2 phase is polycrystalline and dense, 2) the SiC phase is blocky, fine-grained, and often crystallographically-aligned with the Ti_3SiC_2 particles, and 3) the porosity is always in the SiC phase.

The loss of the interpenetrating phase where the SiC-platelets are present throughout the Ti_3SiC_2 phase is a consequence of the hot-press temperature of 1800˚C. This is not a desirable outcome but the tradeoff is seen in the densities. For example, the sample shown in Fig. 4 pressed at 1550˚C has a density of 2.6 g/cm^3 while the sample shown in Fig. 5 and pressed at 1800˚C has a density of 3.8 g/cm^3. The sample in Fig. 6 has a density of 3.83 g/cm^3, which is quite good.

The EDS data for the specimens listed in Table 2 is provided as an average for the SiC phase and for the Ti_3SiC_2 phase for all the samples as Si:C is 1.01:0.99 for the SiC phase and as Ti:Si:C is 2.7:1.0:2.57 as shown in Table 3 using atomic percentages. This is good evidence for having formed the desired phases but the XRD data is the critical data for confirming the phase mixture.

Table 3. Average of EDS data for SiC and Ti_3SiC_2 phases from SEM data

Phase	Ti (atomic %)	Si (atomic %)	C (atomic %)
SiC	0	50.1	49.8
Ti_3SiC_2	43.1	15.9	41.0

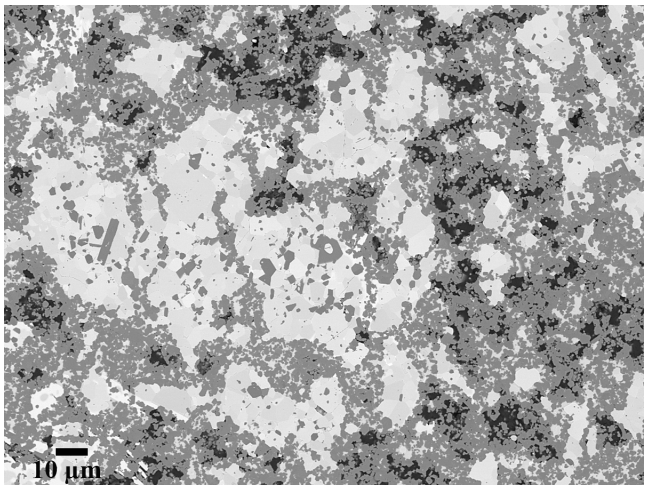

(a)

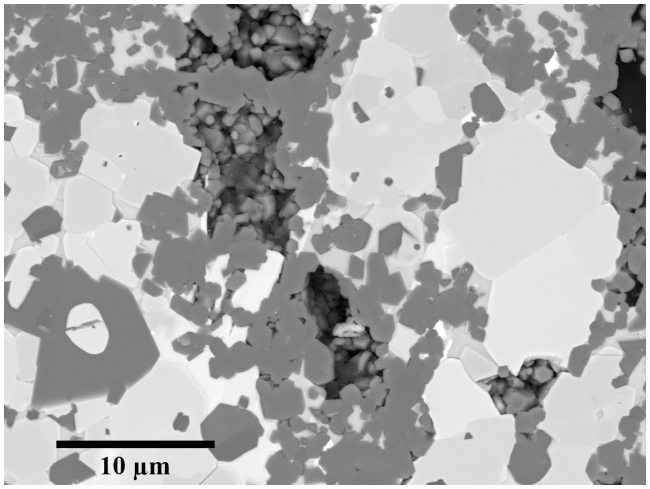

(b)

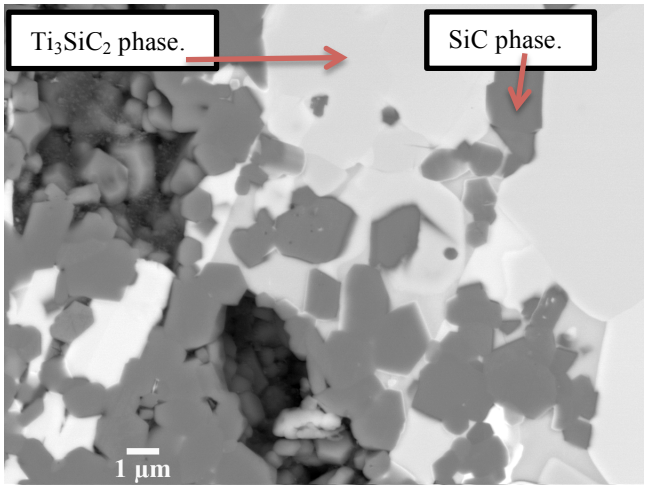

(c)

Figure 6. SEM images of a SiC-alloy hot pressed at 1800˚C (2073 K) and 20 MPa pressure from SiC-filled polymer plus Si + TiC powders at 63% powder loading. The white phase is the Ti_3SiC_2 phase and the darker grey phase is SiC. Note that the pores are contained entirely within the SiC phase.

3.3 X-ray Diffraction (XRD)

The data from XRD taken using Cu-K radiation is shown in Figure 7 for each of the samples listed in Table 2. All of these samples were hot-pressed for 2 hours at 1800˚C (2073 K) at 20 MPa under vacuum and all had densities above 3.65 g/cm^3. This data confirms the phase formation deduced from the SEM and OM images.

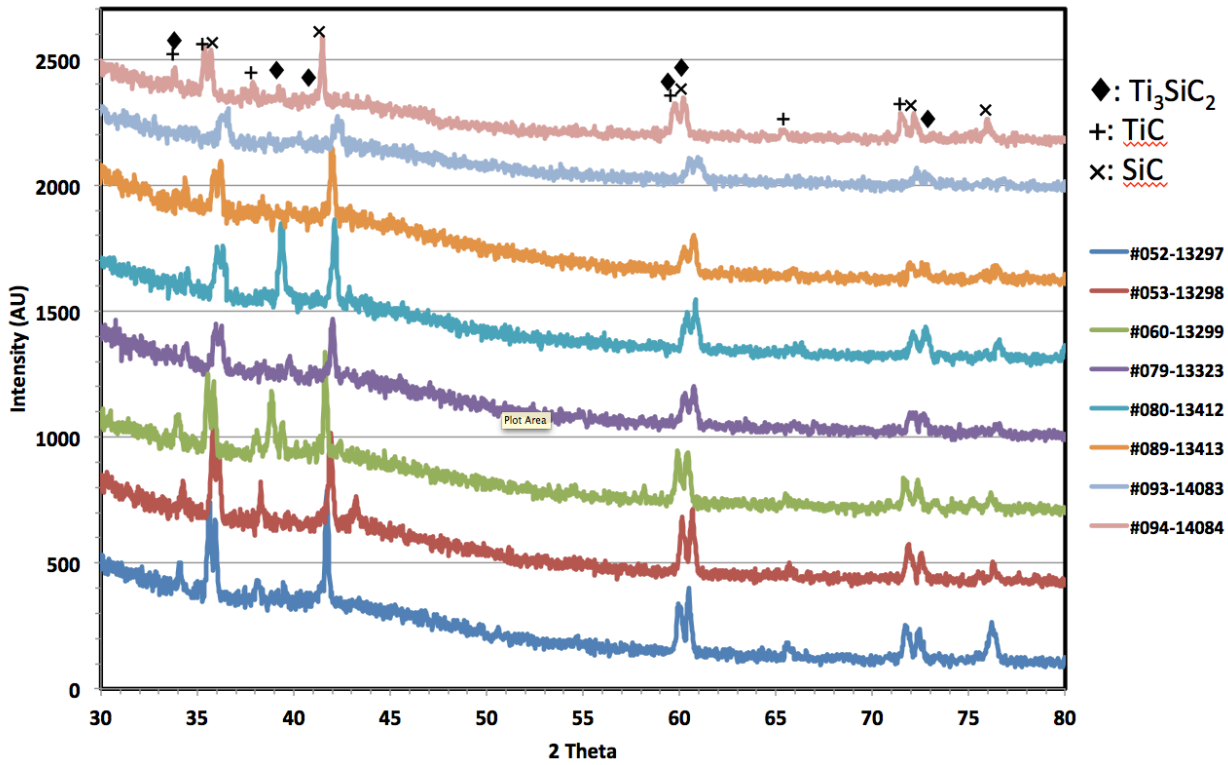

Figure 7. XRD data from each of the samples listed in Table 2. Residual TiC is observed in some of the samples but the major phases are SiC and Ti_3SiC_2 as shown.

3.4 Density

Sample density was measured using the entire hot-pressed disk or, if the disk had cracked, as big a piece of the disk as possible. The densities were determined using Archimedes method with a system that uses a high specific gravity fluid and high-precision balances to achieve a total measurement accuracy of 4 significant figures. Steady progress has been made in increasing the final density into the 3.8-g/cm^3 range. The two samples labeled 093 and 094 were prepared using catalytic amounts of DCP and DVB and this data is not quite understood yet.

3.5 Thermal Conductivity

Thermal conductivities are measured from 25˚C to 500˚C (300 to 773 K) in vacuum using a commercial laser flash thermal diffusivity instrument. The hot-pressed disks are cleaned and polished to remove the graphite paper residue and provide a consistent surface finish for these measurements. The data for all the samples is shown with values at 25˚C, 300˚C, and 500˚C included in Table 2 along with calibration data for Hexoloy SiC that agrees very well with published data for that material. Consistent

with phonon-dominated heat flow in SiC-based materials, the measured thermal conductivity for Hexoloy decreases with increasing temperature. Hexoloy SiC is used as a standard and is tested with each sample to ensure that the instrument is maintaining its accuracy over time and the Hexoloy SiC data has been very consistent over the past year.

Literature data for thermal conductivity of Ti_3SiC_2 indicates that it exhibits weak temperature dependence with decreasing conductivity with increasing temperature and it ranges from about 37 W/m•K at room temperature (300 K) to 35 W/m•K at 500˚C (773 K) [38, 39]. Since the conductivity of SiC is higher than that for Ti_3SiC_2 it is observes, as by others, that compositing with SiC increases the conductivity. Since the conductivity of SiC is also a function of grain size and an average grain size has not yet determined for these materials it is not yet possible to accurately estimate the contribution that SiC makes to the thermal conductivity but the data does show that some of the samples exhibit an increased conductivity compared to polycrystalline Ti_3SiC_2. In fact, the data, with the exception of the room temperature data, is quite consistent with the data of others in the literature for SiC/Ti_3SiC_2 as shown in Figure 8. It is observed that the thermal conductivity values for the materials synthesized here fall into the range expected for a composite of Ti_3SiC_2 and SiC [38, 39] but the data show a slight increase in thermal conductivity with increasing temperature in contrast to what is expected. At the present time the cause of this discrepancy is not understood but it must be noted that it is a real and consistent trend in the data. Values range from 36 W/m•K at 25˚C to 40 W/m•K at 500˚C. The highest values produced are for Sample 060 with 49 W/m•K at 25˚C, 63 W/m•K at 300˚C, and 60 W/m•K at 500˚C, which is quite respectable conductivity for a composite material consisting of SiC/Ti_3SiC_2 [38, 39].

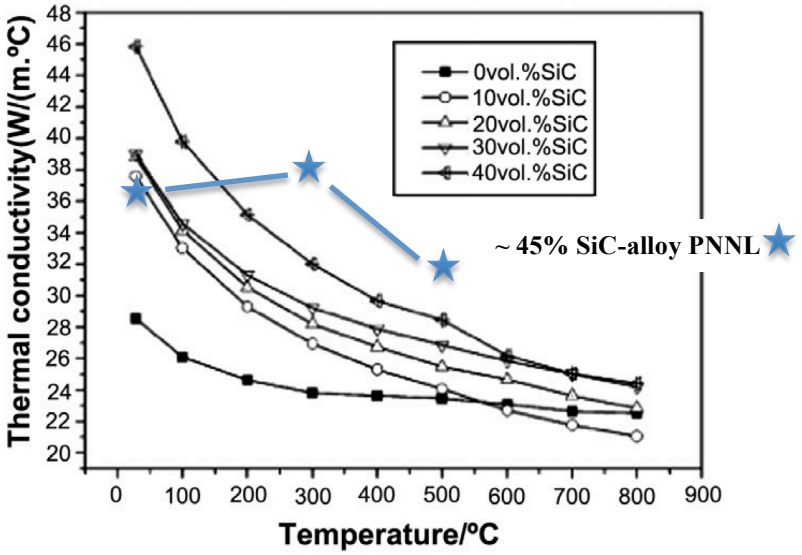

Figure 8. Thermal conductivity data from Ref. [38] showing the effects of adding SiC to Ti_3SiC_2 to increase its thermal conductivity. PNNL average thermal conductivity data for the six nominally identical specimens in Table 2 is shown in blue on this graph and corresponds quite well with this published data at higher temperatures.

3.6 Fracture Toughness

The measured fracture toughness data is shown in Figure 9 as determined using the indentation fracture toughness method following the generally accepted methodology as outlined in Ref. [40]. The

fracture toughness data for the 8 samples listed in Table 2 is shown in Figure 9 along with the data for Hexoloy SiC and their standard errors, respectively. As is evident, additions of Ti_3SiC_2 to SiC generally increase the fracture toughness but only nominally as has been noted before. Similar to the thermal conductivity data shown here, these toughness results are also consistent with literature data for fracture toughness of SiC/Ti_3SiC_2 composites prepared by other methods [38].

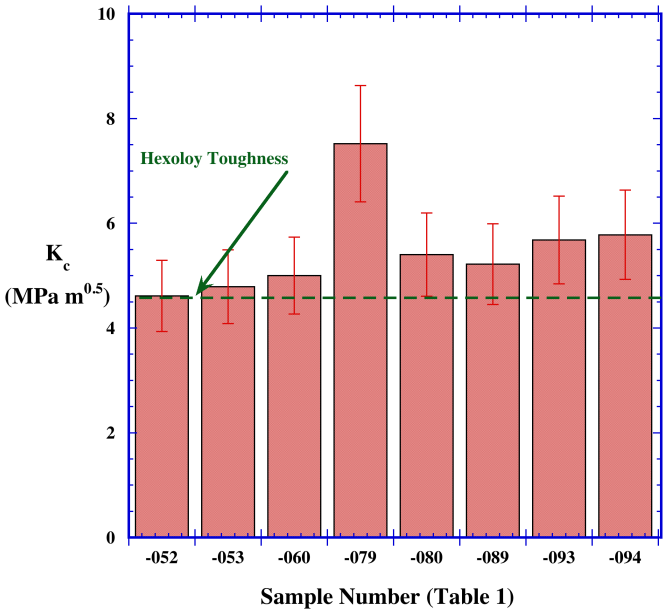

Figure 9. Measured fracture toughness from each of the samples from Table 2 as determined using the indentation fracture toughness method. Ten indents were used for each data point shown in the figure. All of the samples showed an increase in toughness as compared to Hexoloy SiC, which was also tested in this dataset. The dashed green line shows the Hexoloy toughness.

4.0 Conclusions

This brief report documents the synthesis of SiC-based alloys with the general structure of SiC/Ti_3SiC_2 dual phase composites formed by simultaneous polycarbosilane pyrolysis and Si + TiC displacement reactions. To the best of our knowledge these are the first such dual phase composites made by combining these two methods. Data for thermal conductivity and fracture toughness indicate that properties of these composites are in agreement with what others have measured for similar materials that have been synthesized by different methods, such as spark plasma sintering, for example. This is a positive result and indicates that the polymer pyrolysis methods can be used to combine in situ displacement reactions with CNT mats to make tougher composites than can be synthesized by combining SiC and Ti_3SiC_2 materials alone.

However, it must be noted that the synthesis methods used here have not yet been optimized and that some of the correlations that were expected to be helpful in guiding these synthesis efforts are lacking. For example, the porosity of the hot-pressed materials developed here continues to be significant even at 1800˚C (2073 K) and 20 MPa pressure. This result is unexpected and may further limit achievable properties unless fully dense materials can be synthesized. The porosity adds to the inhomogeneity of the materials and increases the variability in measured properties.

For example, as shown in Figure 10, there is a noted lack of correlation between measured density and thermal conductivity, which is unexpected given the known effects of porosity on thermal

conduction. The variability in thermal conductivity seen in Figure 10 indicates that some other material variable, perhaps percolation through one of the phases, is determining the thermal properties. If there were a strong correlation between density and thermal conductivity then the phase volume fractions could be adjusted to tune the conductivity and fracture toughness to optimum values.

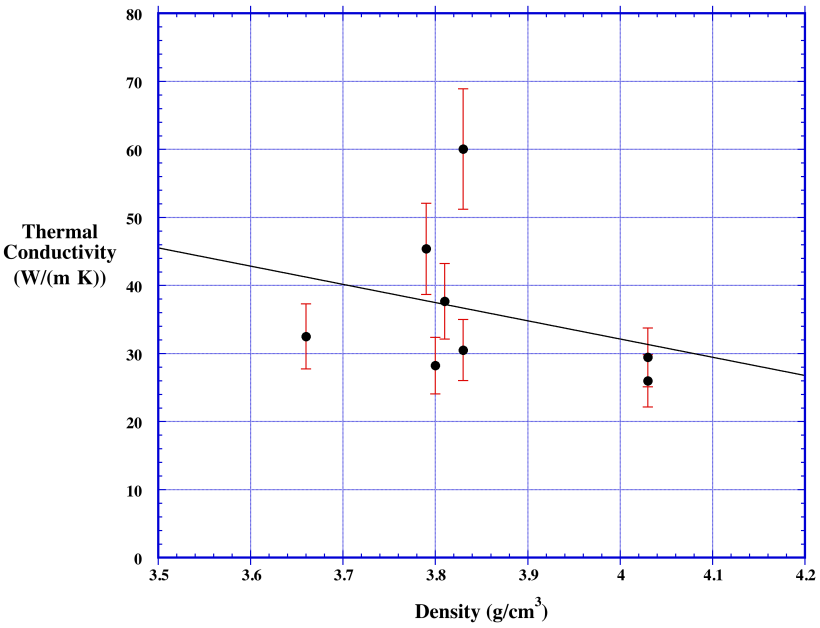

Figure 10. Plot of thermal conductivity as a function of sample density. There is a slight negative correlation between density and conductivity that is unexpected. For the most part, however, this plot shows a lack of a strong correlation since the fitted line has a correlation factor less than 0.3.

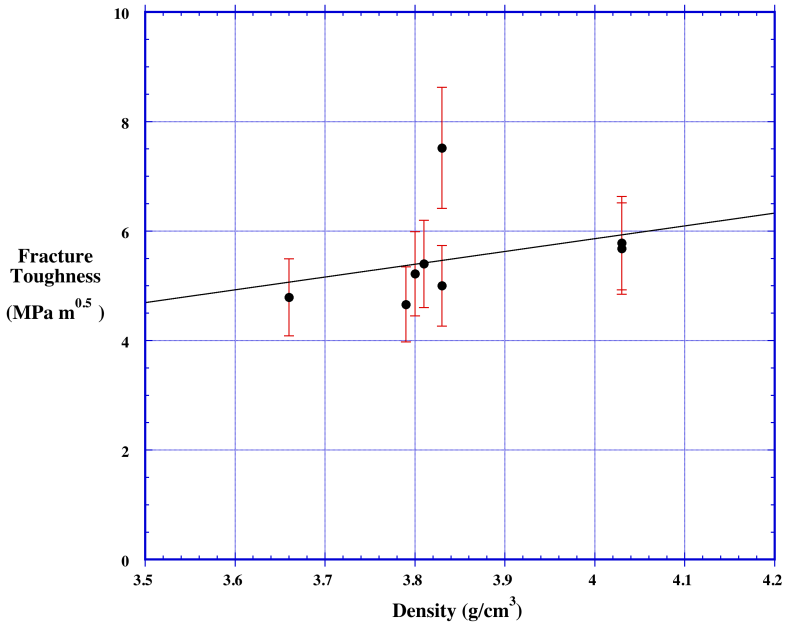

Figure 11. Plot of fracture toughness (indentation method) as a function of sample density. Compared to the lack of correlation for the thermal data this dataset does indicate a general improvement of toughness with increasing density, which would be expected as porosity is decreased.

As is shown in Figure 11, fracture toughness data does show a better correlation with density as increased sample density is positively correlated with an improvement in fracture toughness, which is expected. As porosity is decreased mechanical properties will improve. The fracture toughness data presented here, along with a model data for CNT toughening [41], also suggests that appreciable increases in fracture toughness cannot be achieved using either compositing fabrication as shown in this report or by homogeneously adding CNTs to such a dual phase composite. Rather, this research demonstrates that additional toughening is required and that the development of CNT textured mats must be pursued.

5.0 References

1. Nozawa, T., T. Hinoki, A. Hasegawa, A. Kohyama, Y. Katoh, L.L. Snead, C.H. Henager Jr., and J.B.J. Hegeman, "Recent advances and issues in development of silicon carbide composites for fusion applications," Journal of Nuclear Materials, 2009, 386-388(C), 622-627.
2. Katoh, Y., L.L. Snead, C.H. Henager Jr., A. Hasegawa, A. Kohyama, B. Riccardi, and H. Hegeman, "Current status and critical issues for development of SiC composites for fusion applications," Journal of Nuclear Materials, 2007, 367-370 A(SPEC ISS), 659-671.
3. Zinkle, S.J., "Advanced materials for fusion technology," Fusion Engineering and Design, 2005, 74(1-4), 31-40.
4. Jones, R.H., L. Giancarli, A. Hasegawa, Y. Katoh, A. Kohyama, B. Riccardi, L.L. Snead, and W.J. Weber, "Promise and challenges of SiC_f/SiC composites for fusion energy applications," Journal of Nuclear Materials, 2002, 307-311(2 SUPPL), 1057-1072.
5. Riccardi, B., P. Fenici, A. Frias Rebelo, L. Giancarli, G. Le Marois, and E. Philippe, "Status of the European R&D activities on SiC_f/SiC composites for fusion reactors," Fusion Engineering and Design, 2000, 51-52, 11-22.
6. Kurtz, R.J., R.H. Jones, E.E. Bloom, A.F. Rowcliffe, D.L. Smith, G.R. Odette, and F.W. Wiffen, "Progress in the United States programme to develop low activation structural materials for fusion," Nuclear Fusion, 1999, 39, 2055-2061.
7. Jones, R.H., L.L. Snead, A. Kohyama, and P. Fenici, "Recent advances in the development of SiC/SiC as a fusion structural material," Fusion Engineering and Design, 1998, 41(Pt B), 15-24.
8. Rowcliffe, A.F., E.E. Bloom, R.H. Jones, D.J. Smith, F.W. Wiffen, and W.R. Johnson, "The U.S. program to develop structural materials for near- and long-term fusion systems," Fusion Energy, 1997, 3.
9. Snead, L.L., R.H. Jones, A. Kohyama, and P. Fenici, "Status of silicon carbide composites for fusion," J. Nucl. Mater., 1996, 233-237(Pt. A), 26-36.
10. Sharafat, S., R.H. Jones, A. Kohyama, and P. Fenici, "Status and prospects for SiC-SiC composite materials development for fusion applications," Fusion Engineering and Design, 1995, 29(pt C), 411-420.
11. Hollenberg, G.W., C.H. Henager, G.E. Youngblood, D.J. Trimble, S.A. Simonson, G.A. Newsome, and E. Lewis, "The effect of irradiation on the stability and properties of monolithic silicon carbide and SiC_f/SiC composites up to 25 dpa," Journal of Nuclear Materials, 1995, 219, 70-86.
12. Henager Jr., C.H. and R.J. Kurtz, "Compatibility of interfaces and fibers for SiC-composites in fusion environments," Journal of Nuclear Materials, 2009, 386-388(C), 670-674.
13. Snead, L.L., T. Nozawa, Y. Katoh, T.-S. Byun, S. Kondo, and D.A. Petti, "Handbook of SiC properties for fuel performance modeling," Journal of Nuclear Materials, 2007, 371(1-3), 329-377.
14. Katoh, Y. and L. Snead, "Operating temperature window for SiC ceramics and composites for fusion energy applications," Fusion Science and Technology, 2009, 56(2), 1045-1052.
15. Villmow, T., S. Pegel, A. John, R. Rentenberger, and P. Pötschke, "Liquid sensing: Smart polymer/CNT composites," Materials Today, 2011, 14(7-8), 340-345.
16. Henager, C.H.J., Y. Shin, Y. Blum, L.A. Giannuzzi, B.W. Kempshall, and S.M. Schwarz, "Coatings and joining for SiC and SiC-composites for nuclear energy systems," Journal of Nuclear Materials, 2007, 367-370(1), 1139-43.
17. Radhakrishnan, R., C.H. Henager Jr., J.L. Brimhall, and S.B. Bhaduri, "Synthesis of Ti_3SiC_2/SiC and $TiSi_2$/SiC composites using displacement reactions in the Ti-Si-C system," Scripta Materialia, 1996, 34(12), 1809-1814.
18. Li, J.-F., W. Pan, F. Sato, and R. Watanabe, "Mechanical Properties of Polycrystalline Ti_3SiC_2 at Ambient And Elevated Temperatures," Acta Materialia, 2001, 49, 937–945.

19. Da, C., K. Shirato, M.W. Barsoum, T. El-Raghy, and R.O. Ritchie, "Cyclic fatigue-crack growth and fracture properties in Ti_3SiC_2 ceramics at elevated temperatures," Journal of the American Ceramic Society, 2001, 84(12), 2914-20.
20. Zhou, Y., Z. Sun, and B. Yu, "Microstructure of Ti_3SiC_2 prepared by the in-situ hot pressing/solid-liquid reaction process," Zeitschrift fuer Metallkunde, 2000, 91(11), 937-941.
21. Gilbert, C.J., D.R. Bloyer, M.W. Barsoum, T. El-Raghy, A.P. Tomsia, and R.O. Ritchie, "Fatigue-crack growth and fracture properties of coarse and fine-grained Ti_3SiC_2," Scripta Materialia, 2000, 42(8), 761-767.
22. Farber, L., M.W. Barsoum, A. Zavaliangos, and T. El-Raghy, "Dislocations and stacking faults in Ti_3SiC_2," Journal of the American Ceramic Society, 1998, 81(6), 1677-1681.
23. Yu, H., X. Zhou, W. Zhang, H. Peng, C. Zhang, and K. Sun, "Properties of carbon nano-tubes-C_f/SiC composite by precursor infiltration and pyrolysis process," Materials and Design, 2011, 32(6), 3516-3520.
24. Zhou, T., X. Wang, X. Liu, and D. Xiong, "Improved thermal conductivity of epoxy composites using a hybrid multi-walled carbon nanotube/micro-SiC filler," Carbon, 2010, 48(4), 1171-1176.
25. Yang, K. and M. Gu, "Enhanced thermal conductivity of epoxy nanocomposites filled with hybrid filler system of triethylenetetramine-functionalized multi-walled carbon nanotube/silane-modified nano-sized silicon carbide," Composites Part A: Applied Science and Manufacturing, 2010, 41(2), 215-221.
26. Thostenson, E.T., R. Zhifeng, and C. Tsu-Wei, "Advances in the science and technology of carbon nanotubes and their composites: a review," Composites Science and Technology, 2001, 61(13), 1899-912.
27. Jiang, W., H. Wang, I. Kim, I.T. Bae, G. Li, P. Nachimuthu, Z. Zhu, Y. Zhang, and W.J. Weber, "Response of nanocrystalline 3C silicon carbide to heavy-ion irradiation," Physical Review B (Condensed Matter and Materials Physics), 2009, 80(16), 161301 (4 pp.).
28. Jiang, W., H. Wang, I. Kim, Y. Zhang, and W.J. Weber, "Amorphization of nanocrystalline 3C-SiC irradiated with Si+ ions," Journal of Materials Research, 2010, 25(12), 2341-2348.
29. Jiang, W., L. Jiao, and H. Wang, "Transition from irradiation-induced amorphization to crystallization in nanocrystalline silicon carbide," Journal of the American Ceramic Society, 2011, 94(12), 4127-4130.
30. Henager Jr., C.H., J.L. Brimhall, and J.P. Hirth, "Synthesis of a MoSi2/SiC composite in situ using a solid state displacement reaction between Mo2C and Si," Scripta Metallurgica et Materialia, 1992, 26(4), 585-589.
31. Katoh, Y., L.L. Snead, T. Cheng, C. Shih, W.D. Lewis, T. Koyanagi, T. Hinoki, C.H. Henager Jr., and M. Ferraris, "Radiation-tolerant joining technologies for silicon carbide ceramics and composites," Journal of Nuclear Materials, 2014(0).
32. Katoh, Y., L.L. Snead, C.H. Henager, Jr., T. Hinoki, M. Ferraris, and S.T. Gonczy, "Joining Silicon Carbide for Advanced LWR Fuel Cladding," in 2012 Winter Meeting, 11-15 Nov. 2012. 2012. USA: American Nuclear Society.
33. Henager, J., Charles H. and R.J. Kurtz, "Low-activation joining of SiC/SiC composites for fusion applications," Journal of Nuclear Materials, 2011, 417(1-3), 375-378.
34. Henager Jr., C.H., Y. Shin, Y. Blum, L.A. Giannuzzi, B.W. Kempshall, and S.M. Schwarz, "Coatings and joining for SiC and SiC-composites for nuclear energy systems," Journal of Nuclear Materials, 2007, 367-370, 1139-1143.
35. Henager, C.H., Jr. and R.H. Jones, "Joining SiC ceramics using displacement reactions," in Ceramics Transactions. 1996. Indianapolis, IN: The American Ceramic Society.
36. Henager, C.H., Jr., J.L. Brimhall, and L.N. Brush, "Tailoring structure and properties of composites synthesized in situ using displacement reactions," Materials Science & Engineering A: Structural Materials: Properties, Microstructure and Processing, 1995, A195 (1-2), 65.

37. Williford, R.E., C.H. Henager Jr., and J.P. Hirth, "Matrix creep accommodation in diffusion controlled phase transformations," Acta Materialia, 1996, 44, 763-773.
38. Jianfeng, Z., W. Ting, W. Lianjun, J. Wan, and C. Lidong, "Microstructure and properties of Ti_3SiC_2/SiC nanocomposites fabricated by spark plasma sintering," Composites Science and Technology, 2008, 68(2), 499-505.
39. Barsoum, M.W., T. El-Raghy, C.J. Rawn, W.D. Porter, H. Wang, E.A. Payzant, and C.R. Hubbard, "Thermal properties of Ti_3SiC_2," Journal of the Physics and Chemistry of Solids, 1999, 60(4), 429-39.
40. Anstis, G.R., P. Chantikul, B.R. Lawn, and D.B. Marshall, "A critical evaluation of indentation techniques for measuring fracture toughness. I. Direct crack measurements," Journal of the American Ceramic Society, 1981, 64(9), 533-8.
41. Nguyen, B.N. and J. Henager C.H, "Mode I Fracture Toughness Prediction for Multiwalled-Carbon-Nanotube Reinforced Ceramics," Journal of the American Ceramics Society, 2014, submitted for publication (in review).

Pacific Northwest
NATIONAL LABORATORY

U.S. DEPARTMENT OF
ENERGY

Proudly Operated by Battelle *Since 1965*

902 Battelle Boulevard
P.O. Box 999
Richland, WA 99352
1-888-375-PNNL (7665)
www.pnnl.gov